Accurate Far-Field Measurement of Wide-Angle Scanning Phased Array Antennas

Hongjun Tang [1] and Xianbao Zheng [2]

[1] Southwest China Institute of Electronic Technology, Chengdu, 610036, China
a_thj@163.com

[2] Nanjing Coral Electronic Equipment Co. Ltd, Nanjing, 210018, China
281591383@qq.co

Abstract ─ This paper presents a new approach to the accurate determination of the far-field (FF) pattern of wide-angle scanning phased array antennas (PAAs) that uses planar near-field (NF) technology. When PAAs are engaged in wide-angle scanning, a finite scanning plane and inaccurate probe compensation can lead to truncation errors. The proposed approach reduces these by rotating the PAA to make its main beam perpendicular to the scanning plane. To verify the effectiveness of the approach, both theoretical calculations and actual measurements were undertaken. The simulated and measured results prove that the proposed method is more accurate than traditional NF technology for a large PAA scanning angle, such as ψ_0=50° and Δ_0=50° (in simulation; 54° when measured).

Index Terms ─ Antenna measurement, planar near-field technology, wide-angle scanning phased array antenna.

I. INTRODUCTION

The effective measurement of antenna technologies [1-4] has always been a key issue. Phased array antennas (PAAs) are antennas that can be electrically controlled to change the direction and shape of the beam. In addition to fifth generation (5G) millimeter-wave mobile terminals [5], PAAs are often required in modern radar applications to provide scanning with spatial coverage over a broader angular range. A prominent concern in the design of PAAs has been to enlarge their scanning angle, so measuring their wide-angle scanning performance has become an important topic of research [6]. Wide-angle scanning PAA measurement technologies are usually applied to either far-field (FF) measurements or near-field (NF) measurements [7-9]. However, individual FF measurements tend to deliver very limited information. NF approaches are therefore commonly used for antenna radiation and RCS measurements. Existing planar NF measurements are also best suited to measuring antennas with pencil-beam characteristics. However, finite scanning surface truncation errors often affect the accuracy of planar NF measurements. For antennas that do not scan the beam and antennas that do not have a large scan angle, there usually needs to be a cutoff at the edge of the planar NF scanning plane, below -40 dB, to minimize the truncation error. When the beam of an antenna under test (AUT) is scanned, a large truncation angle is often required to meet the -40 dB cutoff. Unfortunately, large truncation angles are not always possible during actual measurement processes. Furthermore, when the scanning angle of an AUT is large, there can also be inaccuracies in the calculation of the probe compensation.

Various efforts have been made to try and reduce the truncation errors. The most commonly-used method is to select the most appropriate window function. This will have a smooth taper at the edges of the scan plane [10]. However, this method reduces the extent of the reliable region. An equivalent electric current or magnetic current can be introduced to determine the FF pattern [11], but this method requires certain kinds of a priori information, such as the geometry and position of the antenna. It is also extremely time-consuming for electrically large antennas. Some previously proposed techniques [e.g., 12] have suggested enlarging the reliable angular region, but they increase the complexity of the scanning system by demanding additional measurements of the shape. Recently, band-limited signal extrapolation algorithms have been applied to radiation [13] and RCS measurements [14] in the NF region, so as to reduce the truncation errors. However, these approaches cannot be directly applied to the measurement of wide-angle scanning antennas because most of the energy remains outside the NF scanning plane of the AUT and cannot be ignored.

In this paper, we present a novel method for accurately measuring wide-angle scanning PAAs. Prior to the planar NF measurement, the AUT is rotated by a specific angle so that the main beam is perpendicular to the scanning plane. During NF scanning on the test plane, it is then relatively easy to obtain lower near-field

Submitted On: April 22, 2021
Accepted On: August 11, 2021

https://doi.org/10.47037/2021.ACES.J.360915

truncation levels. After the mathematical transformation introduced in this paper, it is possible to achieve accurate PAA FF measurements.

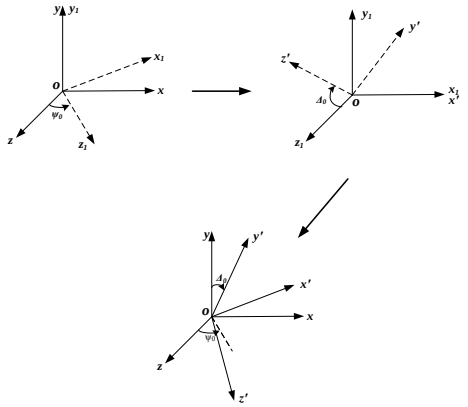

Fig. 1. The relationship between o-xyz and o-x′y′z′.

II. THEORETICAL BACKGROUND

A. Coordinate system transformation

Figure 1 illustrates the relationship between an original coordinate system, *o-xyz*, and a translated coordinate system, *o-x′y′z′*. Assuming that the rotation angles are ψ_0 and Δ_0 in the original coordinate system, we can get the *o-x′y′z′* coordinate system after two rotations. This relationship can be written as:

$$\begin{bmatrix}\hat{x}'\\ \hat{y}'\\ \hat{z}'\end{bmatrix} = T\begin{bmatrix}\hat{x}\\ \hat{y}\\ \hat{z}\end{bmatrix} = \begin{bmatrix}t_{11} & t_{12} & t_{13}\\ t_{21} & t_{22} & t_{23}\\ t_{31} & t_{32} & t_{33}\end{bmatrix}\begin{bmatrix}\hat{x}\\ \hat{y}\\ \hat{z}\end{bmatrix}, \quad (1a)$$

$$\begin{bmatrix}\hat{x}\\ \hat{y}\\ \hat{z}\end{bmatrix} = \begin{bmatrix}t_{11} & t_{21} & t_{31}\\ t_{12} & t_{22} & t_{32}\\ t_{13} & t_{23} & t_{33}\end{bmatrix}\begin{bmatrix}\hat{x}'\\ \hat{y}'\\ \hat{z}'\end{bmatrix}, \quad (1b)$$

where

$$t_{11} = cos\,\psi_0, t_{12} = 0, t_{13} = -sin\,\psi_0,$$
$$t_{21} = -sin\,\Delta_0\,sin\,\psi_0, t_{22} = cos\Delta_0, t_{23} - sin\,\Delta_0\,cos\,\psi_0$$
$$t_{31} = cos\Delta_0\,sin\,\psi_0, t_{32} = sin\,\Delta_0, t_{33} = cos\Delta_0\,cos\,\psi_0. \quad (2)$$

Assuming that the coordinates of the vector, $\vec{r}$, in the two coordinate systems are (x, y, z) and (x', y', z'), it can be represented as follows:

$$\vec{r} = [x \quad y \quad z]\begin{bmatrix}\hat{x}\\ \hat{y}\\ \hat{z}\end{bmatrix} = [x' \quad y' \quad z']\begin{bmatrix}\hat{x}'\\ \hat{y}'\\ \hat{z}'\end{bmatrix} = [x' \quad y' \quad z']\begin{bmatrix}t_{11} & t_{12} & t_{13}\\ t_{21} & t_{22} & t_{23}\\ t_{31} & t_{32} & t_{33}\end{bmatrix}\begin{bmatrix}\hat{x}\\ \hat{y}\\ \hat{z}\end{bmatrix}. \quad (3)$$

The relationship between (x, y, z) and (x', y', z') will then be:

$$\begin{bmatrix}x\\ y\\ z\end{bmatrix} = \begin{bmatrix}t_{11} & t_{21} & t_{31}\\ t_{12} & t_{22} & t_{32}\\ t_{13} & t_{23} & t_{33}\end{bmatrix}\begin{bmatrix}x'\\ y'\\ z'\end{bmatrix} = \begin{bmatrix}t_{11}x' + t_{21}y' + t_{31}z'\\ t_{12}x' + t_{22}y' + t_{32}z'\\ t_{13}x' + t_{23}y' + t_{33}z'\end{bmatrix}. \quad (4)$$

Similarly, we can obtain:

$$\begin{bmatrix}x'\\ y'\\ z'\end{bmatrix} = \begin{bmatrix}t_{11} & t_{12} & t_{13}\\ t_{21} & t_{22} & t_{23}\\ t_{31} & t_{32} & t_{33}\end{bmatrix}\begin{bmatrix}x\\ y\\ z\end{bmatrix} = \begin{bmatrix}t_{11}x + t_{12}y + t_{13}z\\ t_{21}x + t_{22}y + t_{23}z\\ t_{31}x + t_{32}y + t_{33}z\end{bmatrix}. \quad (5)$$

Vectors in any direction in space (ψ, Δ) will correspond to the $o - xyz$ coordinate system and (ψ', Δ') will correspond to the $o - x'y'z'$ coordinate system. Any unit vector, $\hat{r}$, can be represented as follows in the two coordinate systems:

$$\hat{r} = [cos\Delta sin\psi \quad sin\Delta \quad cos\Delta cos\psi]\begin{bmatrix}\hat{x}\\ \hat{y}\\ \hat{z}\end{bmatrix}$$
$$\hat{r} = [cos\Delta' sin\psi' \quad sin\Delta' \quad cos\Delta' cos\psi']\begin{bmatrix}\hat{x}'\\ \hat{y}'\\ \hat{z}'\end{bmatrix}$$
$$= [cos\Delta' sin\psi' \quad sin\Delta' \quad cos\Delta' cos\psi']T\begin{bmatrix}\hat{x}\\ \hat{y}\\ \hat{z}\end{bmatrix}. \quad (6)$$

So, the transformation relationship between (ψ', Δ') and (ψ, Δ) will be:

$$\Delta = arcsin\,(t_{22}sin\Delta' + t_{32}cos\Delta' cos\psi')$$
$$\psi = angle((t_{13}cos\Delta' sin\psi' + t_{23}sin\Delta' t_{33}cos\Delta' cos\psi') + j(t_{11}cos\Delta' sin\psi' + t_{21}sin\Delta' + t_{31}cos\Delta' cos\psi')). \quad (7)$$

Similarly, the transformation relationship between (ψ, Δ) and (ψ', Δ') will be:

$$\Delta' = arcsin\,(t_{21}cos\Delta sin\psi + t_{22}sin\Delta + t_{23}cos\Delta cos\psi)$$
$$\psi' = angle((t_{31}cos\Delta sin\psi + t_{32}sin\Delta + t_{33}cos\Delta cos\psi) + j(t_{11}cos\Delta sin\psi + t_{13}cos\Delta cos\psi)). \quad (8)$$

The relationship between $(\hat{\psi}, \hat{\Delta})$ and $(\hat{x}, \hat{y}, \hat{z})$ is thus:

$$\begin{bmatrix}\hat{\psi}\\ \hat{\Delta}\end{bmatrix} = \begin{bmatrix}cos\psi & 0 & -sin\psi\\ -sin\Delta sin\psi & cos\Delta & -sin\Delta cos\psi\end{bmatrix}\begin{bmatrix}\hat{x}\\ \hat{y}\\ \hat{z}\end{bmatrix}, \quad (9)$$

Similarly,

$$\begin{bmatrix}\hat{\psi}'\\ \hat{\Delta}'\end{bmatrix} = \begin{bmatrix}cos\psi' & 0 & -sin\psi'\\ -sin\Delta' sin\psi' & cos\Delta' & -sin\Delta' cos\psi'\end{bmatrix}\begin{bmatrix}\hat{x}'\\ \hat{y}'\\ \hat{z}'\end{bmatrix}, \quad (10)$$

The dot matrix between $(\hat{\psi}, \hat{\Delta})$ and $(\hat{\psi}', \hat{\Delta}')$ can be expressed as:

$$\hat{\psi}\cdot\hat{\psi}' = cos\psi'(t_{11}cos\psi - t_{13}sin\psi)sin\psi'\,(t_{31}cos\psi - t_{33}sin\psi), \quad (11a)$$

$$\hat{\psi}\cdot\hat{\Delta}' = cos\Delta'(t_{21}cos\psi - t_{23}sin\psi) - sin\Delta' cos\psi'\,(t_{31}cos\psi - t_{33}sin\psi) - sin\Delta' sin\psi'(t_{11}cos - t_{13}sin\psi), \quad (11b)$$

$$\hat{\Delta}\cdot\hat{\psi}' = sin\psi'(t_{31}sin\Delta sin\psi - t_{32}cos\Delta + t_{33}sin\Delta cos\psi) - cos\psi' sin\Delta(t_{11}sin\psi + t_{13}cos\psi), \quad (11c)$$

$$\hat{\Delta}\cdot\hat{\Delta}' = sin\Delta' cos\psi'(t_{31}sin\Delta sin\psi - t_{32}cos\Delta + t_{33}sin\Delta cos\psi) - cos\Delta'(t_{21}sin\Delta sin\psi - t_{22}cos\Delta + t_{23}sin\Delta cos\psi) + sin\Delta' sin\psi' sin\Delta(t_{11}sin\psi + t_{13}cos\psi). \quad (11d)$$

B. Pattern transformation

If a PAA is measured in an $o - x'y'z'$ coordinate system, then it must be transformed to an $o - xyz$ coordinate system to obtain its characteristics. The corresponding pattern in the two coordinate systems can be expressed by $(\hat{\psi}, \hat{\Delta})$ and $(\hat{\psi}', \hat{\Delta}')$, respectively:

$$\vec{F} = F_{\psi'}(\psi', \Delta')\hat{\psi}' + F_{\Delta'}(\psi', \Delta')\hat{\Delta}', \quad (12a)$$

$$\vec{F} = F_{\psi}(\psi, \Delta)\hat{\psi} + F_{\Delta}(\psi, \Delta)\hat{\Delta}. \quad (12b)$$

From this, the transformation relationship between the

$o-x'y'z'$ coordinate system's pattern and the $o-xyz$ coordinate system's pattern can be obtained:

$$F_{\psi}(\psi,\Delta)=F_{\psi'}(\psi',\Delta')\left(\hat{\psi}'\cdot\hat{\psi}\right)+F_{\Delta'}(\psi',\Delta')\left(\hat{\Delta}'\cdot\hat{\psi}\right), \quad (13a)$$

$$F_{\Delta}(\psi,\Delta)=F_{\psi'}(\psi',\Delta')\left(\hat{\psi}'\cdot\hat{\Delta}\right)+F_{\Delta'}(\psi',\Delta')\left(\hat{\Delta}'\cdot\hat{\Delta}\right). \quad (13b)$$

In Eqs. (13a) and (13b), $F_{\psi'}\left(\psi',\Delta'\right)$ and $F_{\Delta'}\left(\psi',\Delta'\right)$ can be obtained through measurement, then, by substituting Eqs. (11a-11d) into Eqs. (13a) and (13b), the FF of the PAA can be acquired.

III. SIMULATED AND MEASURED RESULTS

A. Calculated results

In order to assess the effectiveness of the proposed approach, a measurement model was first established. Fig. 2 shows a schematic diagram of the model. The AUT here consisted of $N_x \times N_y$ electric dipole elements. The element intervals were d_x and d_y, respectively, and the amplitude had a -25dB sidelobe Taylor distribution in the direction of the azimuth and a -35dB sidelobe Taylor distribution in the direction of the elevation. The distance between the scan plane and the AUT was d. The reliable angles were θ_x and θ_y, respectively, and the sampling intervals were Δ_x and Δ_y. The details of the parameters are presented in Table 1.

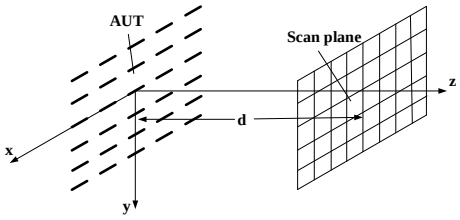

Fig. 2. Schematic diagram of the model.

Table 1: Detailed parameters

Parameter	Value	Parameter	Value
N_x	20	θ_x	60°
N_y	20	θ_y	60°
d_x	0.6λ	Δx	0.4λ
d_y	0.6λ	θy	0.4λ
d	5λ	Antenna Size	12λ×12λ
		Scan Plane Size	29.3×29.3λ

It was assumed that the antenna beam scanning angle was ψ_0=50° and Δ_0=50°, with truncation angles of 60° and 85°, respectively. A comparison of these two cases relating to a normal NF-FF transformation and the theoretical results is shown in Fig. 3. The results show that when the PAA was in a wide-angle scanning mode, the difference between the calculated FF pattern and the theoretical FF pattern decreased as the truncation angle increased. When the truncation angle was 85°, there was an obvious difference between the calculated result and the theoretical result. However, this truncation angle is impossible to realize in actual practice. When the antenna aperture was rotated by ψ=50° and Δ=50°, which was the same as the scanning angle of the PAA, the main beam was orthogonal to the scanning plane. Here, a 60° truncation angle was assumed. As can be seen in Fig. 3 (a), the traditional 60° truncated angle NF-FF was noticeably different from the theoretical FF. Figure 3 (b) shows that they were in good agreement when the truncated angle increased to 85°. However, as can be seen in Fig. 3 (c), the results relating to the proposed method were consistent with the theoretical results when the truncated angle was just 60°. Figure 4 also shows that the calculated results using the proposed method were in good agreement with the theoretical results. This proves the validity and accuracy of the proposed method.

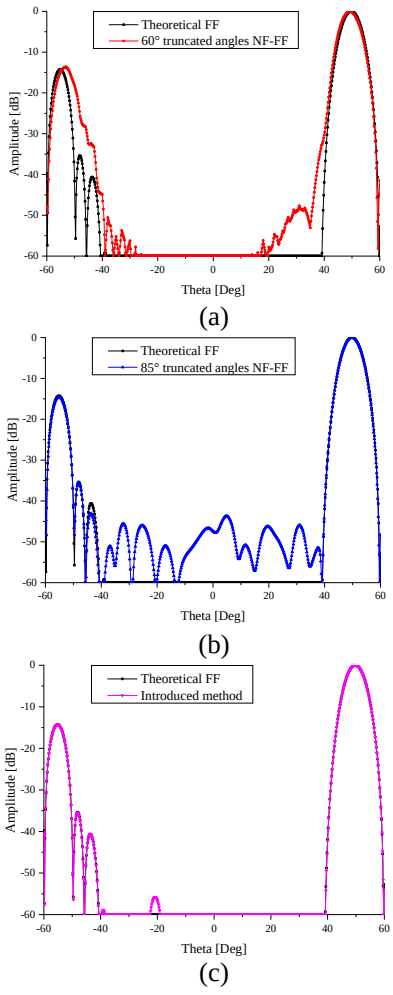

Fig. 3. Comparison between the theoretical results and calculated results for the elevation plane when ψ_0=50°. (a) Comparison between the theoretical FF and a 60° truncated angle NF-FF. (b) Comparison between the theoretical FF and an 85° truncated angle NF-FF. (c) Comparison between the theoretical FF and the proposed method.

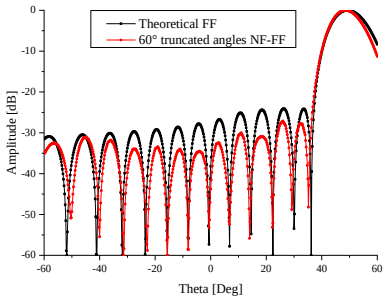

(a)

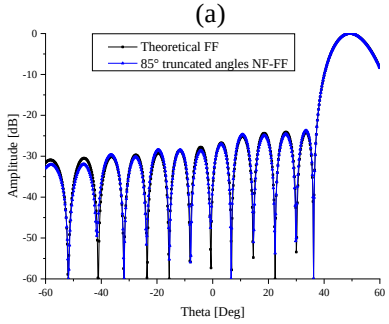

(b)

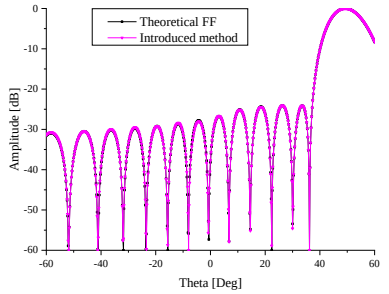

(c)

Fig. 4. Comparison between the theoretical results and calculated results for the elevation plane when Δ_0=50°. (a) Comparison between the theoretical FF and a 60° truncated angle NF-FF. (b) Comparison between the theoretical FF and an 85° truncated angle NF-FF. (c) Comparison between the theoretical FF and the proposed method.

B. Measured results

The proposed method was also used to measure a helix antenna array at 2.2 GHz. This was composed of 2×8 helix antenna elements spaced 85mm apart, with a uniform distribution. It was fed by a one-to-sixteen power divider. The size of the antenna array was 900mm×230mm×110mm, as shown in Fig. 5 (a). Beam scanning at 54° was realized by changing the cable length between the power divider and the radiation element (Fig. 5 (b)). The antenna was rotated so that the main beam was perpendicular to the scanning surface for another planar NF measurement, as shown in Fig. 5 (c). The positional accuracy of the scanning system was 0.05mm and its RMS value was 0.1mm. The 54° scanning angle results shown in Fig. 6 again confirm the effectiveness of the proposed algorithm.

The simulation-based and measured results together serve to confirm that the proposed method is more accurate than using traditional NF technology when the scanning angle of a PAA is large.

(a)

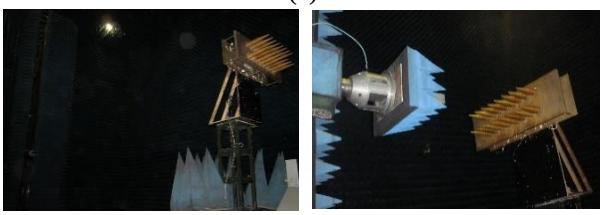

(b) (c)

Fig. 5. The antenna and measurement process: (a) the antenna, (b) conducting the FF measurement, and (c) conducting the NF measurement.

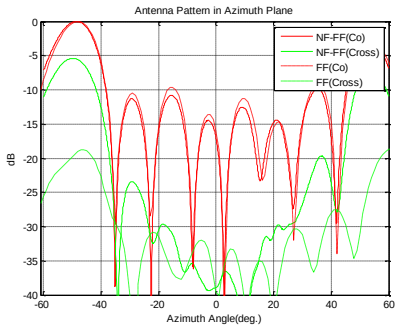

(a)

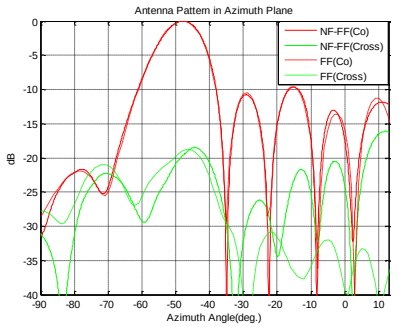

(b)

Fig. 6 Comparison of the NF-FF results and FF results for a 54° scanning angle: (a) using the traditional NF-FF method, and (b) using the proposed method.

IV. CONCLUSION

This paper has presented both theoretical analysis and the real application of an approach that can accurately determine the FF pattern of PAAs based on planar NF technology. Using this approach, it is only necessary to rotate the PAAs, so that the main beam is perpendicular to the scanning plane. The results from both simulations and physical measurements have established the validity of the proposed algorithm. The approach presented in this paper is especially suitable for wide-angle scanning PAAs.

REFERENCES

[1] X. Li, G. M. Wei, L. Yang, and B. Liao, "Fast determination of single-cut far-field pattern of base station antenna at a quasi-far-field distance," *IEEE Trans. Antennas Propag.*, vol. 68, no. 5, pp. 3989-3996, May 2020.

[2] X. Chen, W. Xue, H. Shi, J. Yi, and W. E. I. Sha, "Orbital angular momentum multiplexing in highly reverberant environments," *IEEE Microwave and Wireless Components Letters*, vol. 30, no. 1, pp. 112-115, Jan. 2020.

[3] X. Li, Y. T. Zhang, G. M. Wei, L. Yang, and B. Liao, "Reduction of truncation errors in planar near-field antenna measurements using improved Gerchberg-Papoulis algorithm," *IEEE Trans. Antennas Propag.*, vol. 69, no. 9, pp. 5972-5974, Sep. 2020.

[4] F. Faraz, X. Chen, Q. Li, J. Tang, and X. Zhang, "Mutual coupling reduction of dual polarized low profile MIMO antenna using decoupling resonators," *Applied Computational Electromagnetics Society Journal*, vol. 35, no. 1, pp. 38-43, 2020.

[5] S. Zhang, X. Chen, I. Syrytsin, and G. F. Pedersen, "A planar switchable 3-D-coverage phased array antenna and its user effects for 28-GHz mobile terminal applications," *IEEE Transactions on Antennas and Propagation*, vol. 65, no. 12, pp. 6413-6421, Dec. 2017.

[6] D. Yu, L. Yang, D. M. Fu, and Q. Z. Liu, "Analysis and simulation of system phase errors in planar near-field measurements on ultra-low sidelobe antennas," in *Proc. IEEE ICUWB2010*, pp. 20-23, Sept. 2010.

[7] J. R. Perez and J. Basterrechea, "Particle swarms applied to array synthesis and planar near-field antenna measurements," *Microwave and Optical Technology Letters*, vol. 50, pp. 544-548, Dec. 2007.

[8] X. Chen, "On near-field and far-field correlations in reverberation chambers," *IEEE Microwave and Wireless Components Letters*, vol. 29, no. 1, pp. 74-76, Jan. 2019.

[9] J. R. Perez and J. Basterrechea, "Particle-swarm optimization and finite-difference time-domain (PSO/FDTD) algorithm for multiband and wide-band patch antenna design," *Microwave and Optical Technology Letters*, vol. 44, pp. 398-403, Dec. 2005.

[10] E. B. Joy and C. A. Rose, "Windows 96 for planar near-field measurements," in *Proc. AMTA*, Seattle, WA, pp. 80-85, Oct. 1996.

[11] P. Petre and T. K. Sarkar, "Planar near-field to far-field transformation using an equivalent magnetic current approach," *IEEE Trans. Antennas Propag.*, vol. 40, no. 11, pp. 1348-1356, Nov. 1992.

[12] O. M. Bucci and M. D. Migliore, "A new method for avoiding the truncation error in near-field antennas measurements," *IEEE Trans. Antennas Propag.*, vol. 54, no. 10, pp. 2940-2952, Oct. 2006.

[13] E. Martini, O. Breinbjerg, and S. Maci, "Reduction of truncation errors in planar near-field aperture antenna measurements using the Gerchberg-Papoulis algorithm," *IEEE Trans. Antennas Propag.*, vol. 56, no. 11, pp. 3485-3493, Nov. 2008.

[14] K. T. Kim, "Truncation-error reduction in 2D cylindrical/spherical Near-field scanning," *IEEE Trans. Antennas Propag.*, vol. 58, no. 6, pp. 2153-2158, June 2010.

Hongjun Tang received the M.Sc. degree in Signal and Information Processing from the Institute of Telecommunications Science and Technology, in 2009.

At present, he is engaged in research work in Southwest Institute of electronic technology.

His research interests include array antenna, beam control, and array signal processing.

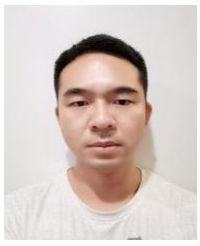

Xianbao Zheng graduated from China Academy of ordnance Sciences, holds a master's degree in Weapon System and Application Engineering. His main research interests include electronic counter-measure system design and interference simulation analysis.